Early Toarcian black shales: a response to an oceanic anoxic event or anoxia in marginal basins?

J.M. McArthur

Department of Earth Sciences, UCL, Gower Street, London WC1E 6BT, UK.

*Corresponding author. E-mail j.mcarthur@ucl.ac.uk

Abstract

The Early Toarcian, organic-rich, black shales of the Cleveland Basin, Yorkshire UK, are the type sediments for the supposed early Toarcian oceanic anoxic event.. The sediments have values of Cd/Mo that are < 0.1 and values of Co(mg/kg) x Mn(%) that are > 0.4. These values are typical of sediment deposited in modern basins that are hydrographically restricted and show that the Cleveland Basin was hydrographically restricted when depositing organic-rich sediments. These palaeo-proxies confirm earlier interpretations, based on Mo/TOC values, that argued for hydrographic restriction. The term Toarcian oceanic anoxic event can now be discarded.

Key words. Toarcian, Mo, Cd, OAE, TOAE, Cleveland Basin, palaeo-proxy

1. Introduction

The Late Pliensbachian and Early Toarcian appear to have been times of considerable environmental change. The changes included a marginally increased rate of faunal extinctions (Raup and Sepkoski 1984; Little and Benton 1995, Cecca and Macchioni 2004; Wignall and Bond 2008), large-scale volcanism (Pálfy and Smith 2000; Guex *et al.* 2016; Percival *et al.* 2018), isotopic variations for several elements incorporated into sediments from seawater, including carbon, (Küspert 1982, Hesselbo *et al.* 2000; McArthur 2007), oxygen in belemnite calcite (McArthur *et al.* 2000; Bailey *et al.* 2003; van de Schootbrugge *et al.* 2005), osmium (Cohen *et al.* 2004) and molybdenum (Pearce *et al.* 2008; Dickson *et al.* 2017), one of the biggest transgressions of the Jurassic (Hallam 1988, 1997), and the deposition of organic-rich shales in marginal basins around the world (Jenkyns 1988 *et seq*. including Jenkyns 2010 and Baroni *et al.* 2018).

The reason why deposition occurred of early Toarcian organic-rich shales (often termed ‘black shales’ even when containing < 5% TOC) has received much attention, although it remains unclear whether this has been because of their visual prominence in outcrop, or because they really did constitute an unusually high proportion of early Toarcian sediments, or because of the accident of geography that placed some into Enlightenment Europe where accessible sections promoted early scientific study. The formation of these sediments has been widely attributed to deposition from an ocean that was globally anoxic (*e.g.* Pearce *et al.* 2008; Thibault *et al.* 2018), where globally is usually taken to mean that all the world's oceans were anoxic (Wignall *et al.* 2010). Others (Hallam 1967, Küspert 1982; Wignall and Hallam 1991; Saelen *et al.* 1996, 1998, 2000; Frimmel *et al.* 2004) have argued that these black shales were deposited in hydrographically restricted basins (enclosed, semi-enclosed, or silled), possibly in response to transgression (Wignall 1991) across basin-and-swell topography. More recently, McArthur *et al.* (2008) used the Mo/TOC-model of Algeo and Lyons (2006) to show that Early Toarcian black shales of the Cleveland Basin (perhaps the type locality) did indeed appear to accumulate in a basin that was restricted hydrographically.

Along with recent studies documenting organic-rich shales in the early Toarcian basinal settings in far-flung localities (*e.g.* Al-Suwaidi *et al.* 2009, 2016; Caruthers *et al*. 2011) has come documentation of early Toarcian sediments that are not organic-rich, especially in western Tethys (Wignall *et al.* 2005; Hesselbo *et al.* 2007; Bodin *et al.* 2010; Baroni *et al.* 2018), thus also calling into question the concept of a globally-anoxic ocean.

Since 2008, new palaeo-proxies have become available to assess depositional environments. The model of Sweere *et al.* (2016), concordant with the observations of Little *et al.* (2015), uses Cd/Mo values, and concentrations of Co and Mn, to differentiate between upwelling and restricted depositional environments. Here, these new palaeo-proxies are applied to the early Toarcian organic-rich shales of the Cleveland Basin to test anew whether they formed under a regime of hydrographic restriction or whether some other model, such as whole-ocean anoxia, or upwelling, is more appropriate.

2. The models

2.1 Mo *v* TOC

The Mo/TOC model of Algeo and Lyons (2006) uses the Mo/TOC value of organic-rich sediment to quantify the degree of hydrographic restriction of a depositional environment. The model rests on the observation that Mo/TOC mass ratios are low (around 6) in modern sediments deposited under severe hydrographic restriction, such as the Black Sea, where renewal times of the water mass are of the order of 1000 to 2000 years (Algeo and Lyons 2006). Low Mo/TOC occurs because Mo is stripped from seawater into sediments, thereby exhausting the Mo supply until the next, infrequent, renewal event. As restriction decreases, the renewal frequency increases and the Mo supply increases until, where euxinia is seasonal and renewal annual, the abundant supply of Mo leads to high values of Mo/TOC in the sediments.

The Mo/TOC model has one drawback; it cannot distinguish between the most extreme variants of its end-members; extreme hydrographic restriction, and the most extreme enhanced upwelling. Both lead to deposition of sediments with low Mo/TOC. For example, Mo/TOC is around 4.5 for sediments from the Black Sea, the archetypal restricted basin, and is around 6 for sediments from offshore Namibia (Algeo and Lyons 2006), a region of extremely enhanced upwelling, where low values occur because the rate of TOC deposition overwhelms the supply of Mo from upwelling.

2.2. Cd *v* Mo

The Cd/Mo proxy of Sweere *et al.* (2016; see also Little *et al.* 2015) is based on the fact that Cd bioaccumulates in phytoplankton whereas Mo does not, so phytoplankton have a Cd/Mo mass ratio > 1. As a consequence, high export of organic matter and Cd, but not Mo, to sediments in upwelling regions creates high sedimentary Cd/Mo. In restricted environments, anoxia/euxinia promotes export of Cd and Mo to the sediments but lower productivity limits plankton-derived export of Cd, leading to Cd/Mo ratios that tend towards the value of 0.006 for seawater. The Cd/Mo model can therefore distinguish between sediments deposited under hydrographically-restricted regimes and those deposited under upwelling regimes, and the fields are separated empirically using a Cd/Mo value of 0.1.

2.3. Co (mg/kg) × Mn (%); Co(EF) × Mn(EF)

This empirical proxy of Sweere *et al.* (2016) uses concentrations of Co (mg/kg) and Mn (%) to assess the degree of restriction of a depositional environment. The proxy name is abbreviated here to Co*Mn when element concentrations are used, and Co(EF)*Mn(EF), where enrichment factor (EF) is used (for a definition, see Section 3.3). These authors noted that restricted environments have Co*Mn > 0.4 whilst unrestricted environments have Co*Mn < 0.4. When use is made of Co(EF) and Mn(EF), restricted environments have values > 1 and unrestricted (upwelling) environments having values < 1. The authors acknowledge that the values 0.4 and 1.0 may need revision in the light of further study. Here, a value of 0.4 is used for both Co*Mn and Co(EF)*Mn(EF), as explained in Section 5.5.

Use of Co and Mn assumes that there are two controls on their supply to sediments. Firstly, both elements have a downward-decreasing vertical profile in the oceans, proving that they are scavenged from the water column into underlying sediments – an hydrogenous supply. In upwelling regions the hydrogenous supply to sediments is low because it is limited by depletion of both elements in upwelled water. Restricted basins usually have an unrestricted, shallow, surface layer that advects laterally, thereby providing potentially more hydrogenous supply. Secondly, in both restricted and upwelling settings, Co and Mn may be remobilized from sediments into the water column where they may be cycled (Brumsack 1989, Neumann *et al.* 1997; Sweere *et al.* 2016). In restricted settings, these remobilized elements cannot escape and eventually are returned to the sediment *via* redox cycling for permanent immobilization; typically, Co in pyrite and Mn in rhodochrosite. (Berrang and Grill 1974; Davison *et al.* 1982; Burdige and Nealson 1986; Sohlenius *et al.* 1996; Neumann *et al.* 1997; Dellwig *et al.* 2010). In open-ocean (unrestricted) settings, such as regions of coastal upwelling, remobilized elements can leak from the system by lateral advection, leading to lower metal enrichments than occurs in the restricted setting, or even to no enrichment over detrital supply.

It is taken here to be trapping efficiency that distinguishes restricted from unrestricted (upwelling) settings, whilst it is acknowledged that the term ‘unrestricted’ usually means ‘upwelling’ as enhanced upwelling is needed to generate TOC-rich sediments in unrestricted environments. The crucial point is whether the depositional environment is ‘leaky’ or is ‘tight’. For example, samples from the Gulf of California, a seasonal-upwelling environment, are suggested by Brumsack (1989) to be low in Mn because of loss from the sediments of Mn remobilized by suboxic diagenesis. They further suggest that Co strongly associates with Mn and so Co may also have been lost. If so, Co and Mn may escape any sediment when the oxic-suboxic interface is at or above the sediment-water interface.

3. Study area

Sedimentary rocks of Early Toarcian age in the Cleveland Basin are exposed well in coastal sections of North Yorkshire, England (Fig. 1). Detailed lithological logs of the sediments, and ammonite zonations, are given by Howarth (1955, 1962, 1973) and its lithostratigraphy by Powell (1984). Ammonite zonations are discussed in Page (2004, 2008) and by Page in Simms *et al*. (2004) where he indicates that the correct name, by nomenclatural priority, for the *Falciferum* Zone in North Yorkshire should be the Serpentinum Chronozone. For continuity with older literature, *Falciferum* Zone is used here.

The sediments are mostly fine-grained mudstones with occasional siltstone intercalations and common carbonate concretions, often in layers that can be traced laterally for many km and act as stratigraphic marker beds. In the Toarcian sediments, numerous lines of concretions occur in the interval from Bed 1 to Bed 32. Beds 33, 35, 37, 42, are particularly prominent rows of carbonate concretions. Bed 39 is a laminated, coccolith-rich, argillaceous limestone some 25 cm in thickness. Bed 40, termed 'The Millstones' by Howarth (1962), is comprised of concretions 2 – 3 m in diameter and a decimetre or two thick that grow upwards from the top of Bed 39. Bed 44 is a line of scatter carbonate nodules, some pyritic. Beds 3, 46 and 50 are sideritic mudstones between 8 and 13 cm. in thickness (Howarth 1973). Bed 48 is a double row of carbonate concretions with some siderite. Three pyrite-rich shales (TS > 5%) occur in the *Tenuicostatum* Zone, the lowest being the Sulphur Band of Chowns (1968) and numbered as Bed 26 of the Cleveland Ironstone Formation (Howarth 1973). It is 15 cm in thickness, and its base marks the traditional base of the *Tenuicostatum* Zone and the base of the Toarcian (Howarth 1973). This positioning, however, does not recognize the fact that first Toarcian ammonite is not recorded until Bed 3 of the overlying Grey Shales Member, around 1.7 m higher (Page, 2003, p.110). Two higher sulphur-rich 'bands', or beds (Beds 2 and 19a of the Grey Shales of Howarth, 1973) are each approximately 20 cm thick and have bases at 1.2 m and 5.0 m above the base of the Toarcian.

In early literature, Beds 33 to 40 inclusive were termed the 'Jet Rock' because they contain an abundance of highly-altered wood (Jet), which takes a high polish and supports a cottage industry in local jewelry-making. In the interval between the upper part of bed 31 and the base of bed 41 (Zone 2, Fig. 2), the water column in the Cleveland Basin was usually euxinic (Schouten *et al.* 2000; Wignall *et al.* 2005). Brief oxygenation events have been documented in the Cleveland Basin by Caswell and Coe (2013) and have been documented in this interval also in the temporally equivalent black-shales of the German Basin (Röhl *et al.* 2001, Schmid-Röhl *et al.* 2002; Frimmel *et al.* 2004; Schwark and Frimmel 2004).

4. Samples and methods

4.1. Samples

Samples from the Cleveland Basin are those of McArthur *et al.* (2008). The samples were collected from exposures at Hawsker Bottoms, Staithes, Port Mulgrave, Saltwick Bay, and Kettleness, on the coast of Yorkshire within a few kilometers of Whitby (Fig. 1; Howarth 1962, 1973). Surficial weathering, which gives the sediment the look of paper shale, was removed to a depth of 5 cm prior to sampling the massive sediment beneath. Stratigraphic levels, measured from the base of the Toarcian, are referred to Hawsker Bottom (Howarth 1955) for Pliensbachian samples, to Port Mulgrave for levels from 0 to 20 m in the Toarcian (Beds 1 to the lower part of Bed 41 of Howarth 1973) and to Saltwick Bay for higher levels (Howarth 1962).

4.2. Chemical analysis

Samples were prepared for analysis by leaching 200 mg samples for two weeks in 2 mls of concentrated HNO_3 without heating, followed by appropriate dilution. Analysis for Mn was done using a Varian 720 ICP-AES. Analysis for Cd, Co, and Mo, was done on a Varian 820 ICP-MS with 30 ml/min He in the reaction cell. For Cd, masses 111, 112, 113, 114, were measured with Te as internal standard. Isobaric interferences from MoO were insignificant. For Co and Mo, internal standards were Ge and Rh respectively, with spiked and unspiked samples being run in pairs to allow for Ge and Rh present naturally. Isobaric interference on Co from Ca needed small correction only for a handful of high-calcite samples. The abundance of $CaCO_3$ was calculated from acid-soluble Ca measured on sediments leached overnight in 1% HNO_3. Data for TS and TOC are from McArthur *et al.* (2008). The results of the analyses are given in Table 1 and are compared to data in Sweere *et al.* (2016) for many world locations and the data of Orani *et al.* (2018) for the Namibian Shelf.

4.3. Enrichment factors

The model of Sweere *et al.* (2016) is applicable only to organic-rich sediments, which are defined here as those containing > 2.5 % TOC. Following Sweere *et al.* (2016), enrichment factors (EFs) are calculated as $[El/Al_{(sample)}] / [El/Al_{(reference)}]$ where the reference is the ‘average shale’ of Wedepohl (1971, 1991; Al 8.8%, Co 19 mg/kg, Mn 850 mg/kg, Mo 2.6 mg/kg). We investigated the effects on data interpretation of using Co(EF) and Mn(EF) rather than concentrations of Co and Mn, and also the effect of using EFs calculated using local normalizers rather than ‘average shale’, as proposed by Böning *et al.* (2004, 2012) and Little *et al.* (2015). Local normalizers for the data in Sweere *et al.* (2016) are based on the minimum El/Al ratios in each data-set. For the new data presented here, the minimum was derived for each sample *via* a polynomial regression of the locally-lowest Co/Al and Mn/Al values within a local window of stratigraphic level.

5. Results

5.1. Element profiles

The stratigraphic profile of concentrations of TOC, TS, Cd, Co, Mn, and Mo are shown on a calcite-free basis in Fig. 2. To aid discussion, the sediment column is divided stratigraphically into Zones 1 to 4 in ascending stratigraphic order. The zones are based on published documentation of the redox state of the water column during sediment deposition and its reflection in sediment composition, notably, but not exclusively, concentrations of TS, TOC, and Mo in the sediments. The boundaries are transitional over several tens of cm, and so defined to a stratigraphic precision no better than ± 20 cm.

The lowermost Zone 1 (− 20 m to + 11.8 m) comprises the sediments from the base of the section to the upper part of Bed 31, in the upper *Tenuicostatum* Zone. In this zone, concentrations of TOC exceed 2.5% only in the three Sulphur Bands (Fig. 2). The water column was oxic excepting for the brief intervals of anoxia or euxinia recorded by the Sulphur Bands. Concentrations of TS are < 3.5%, except in the Sulphur Bands where it is 5 to 8%. Concentrations of Mo are 2 ± 1 mg/kg, excepting in the Sulphur Band proper (0–0.15 m) where concentrations reach 20 mg/kg. In the other Sulphur Bands, the Mo concentration are barely above local background (3.8 mg/kg at 1.19 m and 3.9 mg/kg at 5.11 m).

Zone 2 (11.8 to 21.7 m; euxinic interval) starts in the upper part of Bed 31 in the *Tenuicostatum* Zone and includes the lower 40 cm of Bed 41. It is the ‘interval of maximum restriction’ of McArthur *et al.* (2008). In this interval, the water column was generally euxinic, as shown by the presence of carotenoids in the sediments (Schouten *et al.* 2000) and the small size of pyrite framboids in the sediments (Wignall *et al.* 2005). In this zone, TOC concentrations exceed 2.5% and reach 18% in the mid-*exaratum* Subzone (Beds 33 to 35 inclusive) but decline sharply into Bed 36 whilst remaining > 2.5%. Concentrations of TS are mostly between 4 and 6%, but spike to 9% in Bed 34, about 1 m below the maximum TOC recorded in Bed 35. Concentrations of Mo are around 5 mg/kg.

In Zone 3 (from 40 cm up in Bed 41 to the top of Bed 43; 21.7 m to 35.1 m), concentrations of TOC decrease upwards from 4.6% to 2.6% whilst those of TS are between 2.9% and 4.9 % and concentrations of Mo are high and variable, ranging from 12 to 42 mg/kg. In this zone, the redox condition of the water column is not definitively known. It was interpreted by McArthur *et al.* (2008) to have been mostly euxinic but with a deep redoxcline that varied in level with time and sometimes approached the sediment-water interface.

In Zone 4 (Bed 44 to 50 inclusive; 35.1 to 50.7 m), TOC concentrations are mostly between 2.5 and 3.5% but decline to < 2% at the very top of the section. Concentrations of TOC are > 5% in correlative equivalents (*Bifrons* Zone; Bed 49 and upwards) in some easterly parts of the basin (*e.g.* northern Germany; Jochum 1993; McArthur *et al.* 2008). The concentration of TS is between 1 and

3%, and concentrations of Mo are typically 3 mg/kg, although higher spikes of Mo occur in Bed 49. During the deposition of sediments in this zone, the water-column was probably oxic, given the lowish TOC concentrations in the sediments and the recovery of faunal diversity in this interval (Harries and Little 1999).

With respect to Cd, Mn, and Co, concentrations of Cd are typically 0.3 to 0.4 mg/kg where concentrations of TS are high (Zone 2), and they are similar in Zone 3 where TS is lower. In Zones 1 and 4 they are typically < 0.1 mg/kg. Spikes of Cd concentration of up to 0.8 mg/kg occur (some are arrowed in Fig. 2) and are reproducible on repeat analysis of different subsamples of the same bulk sample. The Sulphur Bands show slight enrichment in Cd.

Concentrations of Mn are mostly 150 to 300 mg/kg but rise to higher in the Sulphur Bands and in Zone 2. Enrichment of Mn is particularly high in Beds 44, 46, 48, and 50. The profile of Co shows a trend of decreasing concentrations upsection on which are superimposed local increases where TS is high, although the increase is minimal in the uppermost of the three Sulphur Bands.

High concentrations of pyrite locally dilute the concentrations of Mn and Mo and high concentrations of calcite locally dilute the concentrations of Co, Cd, and Mn (Table 1). In Zone 1, dilution by pyrite is most pronounced in the Sulphur Bands. In Zone 2, dilution by pyrite is most pronounced in the lower *exaratum* Sz. and by carbonate in Beds 39 and 40, which are ~ 50% calcite.

5.2 Profiles and values of proxies

Stratigraphic profiles of Mo/TOC, Cd/Mo, and Co*Mn are shown in Fig. 3. Values of Mo/TOC are < 1.5 in Zone 2, where TOC is most abundant, and mostly around 6 to 8 in Zone 3, and in the base and top of Bed 49. The high Mo/TOC in the Pliensbachian sediments arises from their low TOC content of < 2% TOC and mostly < 1% (Table 1). Values of Cd/Mo increase up-section in the Toarcian to the top of Zone 2 but remain < 0.1 except in two samples from Zone 2 where they are 0.11 and 0.14 (Table 1) and one sample from the upper part of the second Sulphur Band (Cd/Mo = 0.21). Values of Co*Mn are > 0.4 in Zones 1 to 3, and in Beds 44, 46, 48, 50 in Zone 4, but are < 0.4 in the rest of Zone 4.

5.4. Element associations

Element associations are shown in Fig. 4. Concentrations of Cd, Co, Mn, and Mo, were derived by analysis of sediment leached in concentrated nitric acid and so represent the hydrogenous fraction of the sediment. Concentrations of Co in organic-rich sediments are typically 20 to 50 mg/kg and correlate positively and strongly with TS, positively and less strongly with TOC, and poorly but inversely with

$CaCO_3$. Axial intercepts are < 3 mg/kg Co on the Co *v* TS plot and essentially zero on the Co *v* TOC plot. Manganese correlates weakly and inversely with TS and TOC, and weakly and positively with $CaCO_3$. Cadmium correlates weakly and positively with TOC, TS, and weakly and inversely with $CaCO_3$.

6. Discussion

6.1. The models

For organic-rich sediments, the pathways of Cd, Mn, and Co into sediments have been extensively studied and are summarized by Little *et al.* (2015) and Sweere *et al.* (2016). The trace-element models of Sweere *et al.* (2016) are the more explicit in their use of trace-metal concentrations to determine depositional environment. It is the capacity to estimate the degree of restriction that makes these models useful in an examination of the sediments of the Cleveland Basin: they are not used here to determine redox conditions, as other redox proxies (bioturbation, % TOC, % pyrite, presence/absence of carotenoids) have accomplished this task for the Cleveland Basin.

6.2 Validation

The model of Sweere *et al.* (2016) assumes that Cd, Co, Mn, and Mo, in sediments originate either from detrital or hydrogenous supply. Application of the Cd/Mo and Co*Mn palaeo-proxies thus requires this dual source to apply to the Cleveland Basin. The element associations shown in Fig. 4 show that the Cd, Co, and Mn in the Cleveland Basin are largely hydrogenous in origin.

Cobalt is hosted by pyrite and, to a lesser degree, organic matter. According to Wignall *et al.* (2005), pyrite in the organic-rich shales (Zone 2) was precipitated from euxinic seawater, a finding anticipated by the observation of Gad *et al.* (1969) that most of the Fe in the sedimentary pyrite in OM-rich sediments of the Cleveland Basin derived from seawater.

Cadmium appears to be associated with sulphide and TOC (Figs. 2, 4), showing that in Zones 2 and 3, where Cd, TS, and TOC are highest, the Cd is overwhelmingly hydrogenous, as expected from the geochemical considerations in Sweere et al. (2016).

Concentrations of Mn correlate positively, if weakly, with $CaCO_3$, increasing from an axial intercept of 0.01 % Mn. Concentrations of Mn in the organic-rich sediments of Zone 2 range from 0.03 to 0.09, so most of the Mn in these sediments is hydrogenous in origin. This is no surprise, as numerous studies show that Mn supply to sediments in restricted basins occurs by oxidation to MnO_2, either at the redoxcline or during oxygenating events involving mixings, followed by export to the sediments and probably conversion in the sediments to $MnCO_3$ (*e.g.* Neumann *et al.* 1997; Sohlenius *et al.* 1996).

6.3. Application

The Cd/Mo Proxy: on a plot of Cd *v* Mo (Fig. 5), two samples plot on the border of the restricted field of Sweere *et al.* (2016) whilst the rest plot squarely within it. The values show that the samples formed under a regime of hydrographic restriction. This palaeo-proxy thus confirms this same conclusion based on Mo/TOC ratios (McArthur *et al.* 2008). Sapropels from the eastern Mediterranean, also have Cd/Mo < 0.1 (Fig. 4 of Sweere *et al.* 2016). The sapropels formed beneath a low-salinity surface layer during times of increased run-off from north Africa (Rohling *et al.* 2015). Restriction of circulation in the Cleveland Basin by a low-salinity cap has been postulated repeatedly (Hallam 1967, Wignall 1991, Saelen *et al.* 1996, 1998, 2000; McArthur *et al.* 2008; Dera and Donnadieu 2012); the Cd/Mo values are concordant with that view.

The Co(mg/kg) x Mn(%) Proxy: for the organic-rich sediments of the Cleveland Basin, values of Co*Mn exceed 0.4 in all sediments except the main beds of Zone 4 (Beds 45, 47, 49), confirming the interpretations drawn from the Mo/TOC and Cd/Mo proxies that the organic-rich sediments in Zones 2 and 3 of the Cleveland Basin formed in and environment that was hydrographically restricted. Values of Co*Mn separate sediments in each zone better than do values of Cd/Mo (Fig. 6). The Mo enrichment in Zone 3 was attributed by McArthur *et al.* (2008) to a lessening in this interval of the severe hydrographic restriction present during deposition of sediments in Zone 2. The relative positions of samples from Zones 2 and 3 on Fig. 6 confirm this interpretation, with Zone 3 sediments having lower Co*Mn than samples from Zone 2.

The combined Cd/Mo and Co*Mn proxies (Fig. 6), show that the sediments of the Cleveland Basin accumulated in an hydrographically-restricted environment, as suggested by Hallam (1967), Saelen *et al.* (1996, 1998, 2000) and many others, and confirmed by McArthur *et al.* (2008) using Mo/TOC analysis. The Cd/Mo proxy is particularly compelling, given its strong observational base (Brumsack 1989, Little *et al.* 2015; Sweere *et al.* 2016). Nevertheless, caution is needed in applying these palaeo-proxies to ancient environments.

Mo alone. A control on the Mo concentration in sediments of the Cleveland Basin may be the locus of the redoxcline in relation to the sediment-water interface. McArthur *et al.* (2008) postulated that the concentration of Mo in the sediments of Zone 3, the Mo-rich interval, was governed by the depth of the redoxcline, which in turn governed the size of the euxinic reservoir available to supply Mo to sediments. Scott and Lyons (2012) suggested that, for unrestricted environments, when the redoxcline is at the sediment-water interface and euxinia is confined to pore waters, Mo concentrations will rarely exceed 20 mg/kg. The Mo concentration in Zone 3 is 19 ± 5 mg/kg (1 s.d. excluding two outliers at 34 and 49 mg/kg); that is, most concentrations are at the upper limit identified by Scott and Lyons (2012) for confinement of euxinia to pore water, with only a few levels exceeding the limit. The TOC concentrations in Zone 3 are 3.4 % ± 0.4 %, again excluding the two high-Mo outliers with TOC 4.6% and 3.6% (Table 1).

In Zone 2, the euxinic interval, Mo concentrations are around 5 mg/kg and Mo/TOC around 1. These values are well below those found in the overlying Zone 3. The difference in Mo concentrations between Zones 2 and 3 is likely attributable to degree of hydrographic restriction (McArthur *et al.* 2008). In Zone 2, restriction was almost total, so the sediments sequestered little Mo because little Mo was available in the stagnant water column. In contrast, the lesser restriction (more frequent water renewal) in Zone 3 provided more Mo to supply sediments. The considerations of Scott and Lyons (2012) suggest that that frequency of renewal was sufficient to make the water column largely oxic or anoxic for most of the time, thereby confining euxinia to the pore waters and so limiting Mo supply to diffusion into sediments, except for brief euxinic intervals.

6.4. Caveats

Diagenetic effects: the thin sideritic/calcitic mudstones/concretions of Beds 44, 46, 48 and 50 are particularly rich in Mn (Table 1; Fig. 2) and so plot well into the restricted field. The beds mark hiatuses or slow-downs in sedimentation together with oxygenation of overlying seawater, a combination that allows Mn, mobilized from the sediments by reduction and upward diffusion, to be precipitated at the sediment-water interface or in the sediment a few cm below it. The extreme Mn enrichment, together with the thinness of the beds (a few decimetres), plus other evidence of slow sedimentation at these levels, all mark them as uncharacteristic of Zone 4 generally. The decreased sedimentation associated with these beds is attested to by a high abundance of belemnites associated with each: it was noted by Hallam (1967) that belemnite abundance in these sediments was a proxy for a reduced sedimentation rate, a matter confirmed by personal observation. These beds thus show diagenetic enrichment of Mn. The fact that they plot in the restricted field of Fig. 6 shows a weakness of this palaeo-proxy.

Hydrogenous v detrital: the value of 0.4 for Co*Mn used to separate restricted and unrestricted fields was derived empirically by Sweere *et al.* (2016) from examination of Co*Mn in a range of modern environments (their Fig. 3). The derivation of the value was illustrated by those authors by reference to a plot of Co*Mn *v* Al, which is reproduced in Fig. 7 with the addition of data from the Cleveland Basin. Whilst the derivation of the proxy was aided by Al data, it can be applied, as it is here, without the need for concentrations of Al. Nevertheless, it is interesting to show how the Cleveland Basin data fits on such a plot.

The disposition of samples on Fig. 7 will depend upon the relative contributions of detrital and hydrogenous Co and Mn, and the ratio Co/Mn in both. Where detrital supply dominates (Cariaco Basin, Peru, Namibia, Gulf of California) Co*Mn correlates positively with Al. Where hydrogenous supply dominates, the relation should become inverse as aluminosilicates act more as diluents than contributors to the Co+Mn budget. Curiously, this does not seem to be the case for any modern environment (Fig. 7). It appears to be the case for the Cleveland Basin (Fig. 7) but the effect is more apparent than real, deriving from different Co*Mn and Al in each of zones 1 to 4, as there is no relation between Co*Mn and Al in any of them. Notwithstanding the above, a divider that is approximately horizontal and has a value of 0.4 can be obtained from a binary mixing model that has end-members as follows: detrital Co 13mg/kg, detrital Mn 0.012%; hydrogenous Co 4 mg/kg, hydrogenous Mn 0.013%.

The Case of the Cariaco Basin. This restricted basin renews its water around every 100 years (Deuser 1973). Its Co*Mn values are nevertheless similar to those for the Gulf of California, an environment of seasonal upwelling. The values for both localities plot in the same part of the unrestricted (upwelling) field on Fig. 7. For the Cariaco Basin, this appears to be at odds with the fields delineated by Sweere *et al.* (2016; the discrepancy remains when Co(EF)*Mn(EF) is plotted, see Fig. 8). A reconciliation is possible: the supply into the Cariaco Basin of trace elements from hydrogenous and biogenic sources is largely controlled by seasonally-variable upwelling (Piper and Dean 2002), so upwelling is a common characteristic of these two areas.

A small subset of the Cariaco data (5.37 to 6.02 m depth, core PL07-39PC of Piper and Dean, 2002) have values that spread into the restricted field of the Co*Mn (and CoEF*MnEF) proxies. Values of Mn/Al and Co/Al in this depth interval form well-defined peaks rising to twice background values. The Mn enrichment is attributed by Piper and Dean (2002) to oxic trapping of diagenetically-remobilized Mn from underlying sediments (*cf.* the interbeds 44, 46, 48, 50 of Zone 4 in the Cleveland Basin). Another explanation is possible. The enriched sediments were laid down during the glacial to interglacial transition (14.8 ka to 11.5 ka) when salinity in the North Atlantic and Gulf of Mexico was lowered by Meltwater Pulse 1A (Fairbanks 1989). The presence of a low-salinity layer would have restricted the basin and lead to less leakage of trace elements by remobilization from the sediments. If so, sediments laid down in the Cariaco Basin during Meltwater Pulse 1B (2.90 to 3.60 m depth) should also show an enrichment of Mn/Al and Co/Al, and indeed they do, although the degree of enrichment is lower than during Meltwater Pulse 1A.

These Mn-enriched intervals in the Cariaco Basin plot with samples from the Baltic Sea, where euxinic basins (Arkona, Bornholm, Gotland, deeps) have a low salinity surface layer, and with the Black Sea, which also has a low-salinity surface layer. If indeed the Mn and Co enrichments can be attributed to a low-salinity surface layer over the Cariaco Basin as a result of meltwater freshening of the surface mixed layer, the Co*Mn proxy may be informing us of the nature of the mechanism by which a basin becomes restricted – isolation by a pycnocline, rather than by a thermocline.

Other anomalies include the fact that samples from the Black Sea, where deep-water renewal times are 1000-2000 years, plot with samples from the Bornholm Basin, where renewal times are ten or more times less; nevertheless, both are restricted basins. Samples from the Arabian Sea (unrestricted, upwelling) overlap slightly with samples from the Arkona Deep of the Baltic Sea but do not overlap with samples from the Bornholm Deep or with samples from the Gotland Deep of the Baltic Sea (data of Neumann *et al.* 1997) which, for clarity of presentation, are not shown on Fig. 7 owing to their extreme enrichment in Mn (concentrations of 2 to 5%). In the Baltic, the enrichment in Mn and Co*Mn increases as distance from the open ocean increases (Fig. 7 and data of Neumann *et al.* 1997) and is, presumably, either a measure of the frequency and degree of seawater penetration or a measure of the effectiveness of the surface low-salinity layer in isolating the deeps (Neumann *et al.* 1997; Sohlenius *et al.* 1996, 2001; Scholz *et al.* 2018, refs therein).

6.5. The Co(EF) x Mn(EF) proxy

6.5.1. Field dividers

As an alternative to the use of Co*Mn, Sweere *et al.* (2016) propose the use of Co(EF)*Mn(EF) with a fixed value of 1.0 as a field divider between restricted and unrestricted environments (Fig. 8). The value of 1.0 applies only when no hydrogenous component exists and detrital Co and Mn have Co/Al and Mn/Al ratios equal to those in average shale. The use of a local-shale normalizer may be more appropriate (see next section).

The field-divider of 1.0 is inconsistent with their value of 0.4 for the Co*Mn field-divider (Fig. 7). The inconsistency arises from the fact that CoEF*MnEF includes the term Al^2. Rearranging, Co(EF)*Mn(EF) = (Co*Mn*k)/Al^2 where k = a constant with a value of 47.95, the Al^2/(Co*Mn) value of average shale. So, a plot of Al *v* Co(EF)*Mn(EF) is essentially a plot of Al v 1/Al^2 and must be non-linear with a negative gradient. Recognizing this, the Co*Mn value of 0.4 used by Sweere *et al.* (2016) as a discriminator for Co*Mn (Fig. 7) has been plotted on Fig. 8a, where it is shown as a black dotted curve. A better discriminator than Co(EF)*Mn(EF) might be (Co*Mn)EF; that is $(Co{*}Mn/Al)_{Sample}$ / $(Co{*}Mn/Al)_{Av.\ shale}$. When plotted against Al, however, a non-linear field-divider would still be needed.

When the value of Co*Mn = 0.4 is used as a field-divider on Fig. 8a, the disposition of samples with respect to it is identical to the disposition of samples on Fig. 7 with respect to same field-divider of 0.4 for Co*Mn. No advantage accrues from the use of Co(EF)*Mn(EF) over the use of Co*Mn, and the former has the disadvantage that the field-divider must be non-linear, and have a negative slope, as it would be essentially a graph of Al *v* 1/Al.

6.5.1.Local-Shale normalizers

he discrimination of environments in previous sections is not improved by use of EFs calculated using local normalizers, rather than 'average shale' (Fig. 8b; Böning *et al.* 2012; Little *et al.* 2015; Neumeister *et al.* 2016b). Use of local normalizers increases the separation of the Black Sea, the Baltic Sea, and the Cleveland Basin, from other data but does not improve the discrimination between that other data. It also results in the Arkona Basin plotting directly on the Arabian Sea data. Notwithstanding the above, the samples from the Cleveland Basin plot in the restricted field.

7. Conclusion

The results presented here for both the Cd/Mo proxy and the Co*Mn proxy show hydrographic restriction was a defining feature of black-shale deposition in the early Toarcian of the Cleveland Basin. This result confirms the same finding by McArthur *et al.* (2008) for these sediments through the use of the Mo/TOC proxy of Algeo and Lyons (2006) and contradict the interpretation of Mo/TOC in the Cleveland Basin by Pearce *et al.* (2008) in terms of whole-ocean anoxia. The extremely low Mo concentrations (around 3 - 8 mg/kg) in Zone 2 pose a problem for models invoking whole-ocean anoxia, especially so given the higher Mo and Mo/TOC in the overlying Zone 3, since it is Zone 2, the *exaratum* Sz., that is often viewed as a time of enhanced global weathering. Were that so, the supply of Mo to the oceans would be greater in Zone 2 than in the overlying Zone 3, where Mo concentrations are higher.

The idea of hydrographic restriction in the Early Toarcian Cleveland basin has been invoked repeatedly to explain the deposition of its organic-rich sediments (citations in this work), and for other parts of the early Toarcian of NW Europe: the Paris Basin (Lézin *et al*. 2013), the German Basin (Frimmel *et al.* 2004), and the Austrian Tyrol (Neumeister *et al.* 2016a,b). More recently, Dickson *et al.* (2017) interpreted differences from place-to-place across NW Europe of δ^{98}Mo profiles through the early Toarcian black shales as evidence of "*fluctuations in the exchange rate of open ocean seawater with Cleveland Basin water*", echoing the view of McArthur *et al.* (2008) that fluctuations in, *inter alia*, δ^{98}Mo in the Cleveland Basin "*must relate to changes in the rate of deepwater renewal.*". Furthermore, modelling by Baroni *et al.* (2018) of sea-water circulation in the Tethyan Seaway during Toarcian times supports the scenario of regional restriction affecting marginal basins of the northeastern Tethys, possibly as a result of freshwater invasion *via* the Viking corridor (Dera and Donnadieu 2012), whilst southern and western regions of Tethys remained unrestricted. Finally, both Suan *et al.* (2018) and Fantasia *et al.* (2019) reveal substantial variations in the character of sediments in the early Toarcian that they interpret in terms of strong local influences on the deposition of organic matter in Tethyan sediments rather than whole-ocean anoxia.

Using Mo/TOC, Cd. Mo, and Co*Mn, the way is now open for a robust evaluation of the depositional environment of other organic-rich sediments using the combined approach offered by these palaeo-proxies, as it is becoming increasingly clear that the multiple environmental disturbances of early Toarcian times did not include whole-ocean anoxia.

Acknowledgements

Thanks go to Paul Wignall, an anonymous reviewer, and Harilaos Tsikos, for constructive review of the script; to Guillaume Suan for providing a draft of Fig. 1, and to Tom Algeo for providing the aluminium data.

References

Algeo T.J. and Lyons T.W. 2006. Mo–total organic carbon covariation in modern anoxic marine environments: Implications for analysis of paleoredox and paleohydrographic conditions. Paleoceanography, 21, PA1016, doi:10.1029/2004PA001112.

Al-Suwaidi A., Damborenea S., Hesselbo S., Jenkyns H., Manceñido M. and Riccardi A. 2009. Evidence for the Toarcian oceanic anoxic event in the Southern Hemisphere (Los Molles Formation, Neuquén Basin, Argentina). Geochim. Cosmochim. Acta, 73(13), suppl. 1, A33.

Al-Suwaidi A.H., Hesselbo S.P., Damborenea S.E., Manceñido M.O., Jenkyns H.C., Riccardi A.C. , Angelozzi G.N. and Baudin F. 2016. The Toarcian Oceanic Anoxic Event (Early Jurassic) in the Neuquén Basin, Argentina: a reassessment of age and carbon isotope stratigraphy. Jour. Geol., 124, 171–193.

Bailey T. R., Rosenthal Y., McArthur J. M., van de Schootbrugge B. and M. F. Thirlwall (2003), Paleoceanographic changes of the late Pliensbachian– Early Toarcian interval: A possible link to the genesis of an oceanic anoxic event. Earth Planet. Sci. Lett., 212, 307–320,

Baroni I.R., Pohl A., van Helmond N.A.G.M., Papadomanolaki N.M., Coe A.L., Cohen A.S., van de Schootbrugge B., Donnadieu Y. and Slomp C.P. 2018. Ocean circulation in the Toarcian (Early Jurassic): a key control on deoxygenation and carbon burial on the European Shelf. Paleoceanography and Paleoclimatology, 33, 994–1012.

Berrang P.G. and Grill E.V. 1974. The effect of manganese oxide scavenging on molybdenum in Saanich inlet, British Columbia. Marine Chemistry 2, 125–148.

Böning P., Brumsack H., Böttcher M.E., Schnetger B., Kriete C., Kallmeyer J., and Borchers S.L. 2004. Geochemistry of Peruvian near-surface sediments: Geochim. Cosmochim. Acta, 68(21), 4429–4451.

Böning P., Fröllje H., Beck M., Schnetger B. and Brumsack H.-J. 2012. Underestimation of the authigenic fraction of Cu and Ni in organic-rich sediments: Mar. Geol., 323–325, 24–28.

Bodin S., Mattioli E., Fröhlich S., Marshall J.D., Boutib L., Lahsini S. and Redfern J. 2010. Toarcian carbon isotope shifts and nutrient changes from the Northern margin of Gondwana (High Atlas, Morocco, Jurassic): palaeoenvironmental implications. Palaeogeog. Palaeoclimatol. Palaeoecol., 297 377–390.

Burdige D.J. and Nealson K.H. 1986. Chemical and microbiological studies on sulfide-mediated manganese reduction. Geomicrobiol. Jour., 4, 361–387.

Brumsack H.J. 1989. Geochemistry of recent TOC-rich sediments from the Gulf of California and the Black Sea. Geologische Rundschau, 78/3, 851–882.

Caruthers A.H., Gröcke D.R. and Smith P.L. 2011. The significance of an Early Jurassic (Toarcian) carbon-isotope excursion in Haida Gwaii (Queen Charlotte Islands), British Columbia, Canada. Earth Planet. Sci Letters, 307, 19–26.

Caswell B.A. and Coe A.L. 2013. Primary productivity controls on opportunistic bivalves during Early Jurassic oceanic deoxygenation. Geology, 41(11), 1163–1166.

Cecca F. and Macchioni F. 2004. The two Early Toarcian (Early Jurassic) extinction events in ammonoids. Lethaia, 37(1), 35-56.

Chowns T.M. 1968. Environmental and diagenetic studies of the Cleveland Ironstone Formation of north-east Yorkshire. Ph.D. thesis, University of Newcastle upon Tyne. https://theses.ncl.ac.uk/dspace/handle/10443/268

Cohen A.S., Coe A.L., Harding S.M., and Schwark L. 2004. Osmium isotope evidence for the regulation of atmospheric CO_2 by continental weathering. Geology, **32**, 157–160, doi:10.1130/G20158.1.

Davison W., Woof C. and Rigg E. 1982. The dynamics of iron and manganese in a seasonally anoxic lake; direct measurement of fluxes using sediment traps. Limnol. Oceanogr. 27(6), 987–1003.

Dellwig O., Leipe T., März C., Glockzin M., Pollehne F., Schnetger B., Yakushev E.V., Böttcher M.E.and Brumsack H.-J. A new particulate Mn–Fe–P-shuttle at the redoxcline of anoxic basins. Geochim. Cosmochim. Acta 74, 7100–7115.

Deuser W.G. 1973. Cariaco Trench—oxidation of organic matter and residence time of anoxic water: Nature, 242, 601–603.

Dera G., Pellenard P., Neige P., Deconinck J-F., Pucéat E. and Dommergues J.L. 2009. Distribution of clay minerals in Early Jurassic Peritethyan seas: palaeoclimatic significance inferred from multiproxy comparisons. Palaeogeography, Palaeoclimatology, Palaeoecology 271, 39–51.

Dera G. and Donnadieu Y. 2012. Modeling evidences for global warming, Arctic seawater freshening, and sluggish oceanic circulation during the Early Toarcian anoxic event. Paleoceanography, 27, PA2211, doi:10.1029/2012PA002283.

Dickson A.J., Gill B.C., Ruhl M., Jenkyns H.C., Porcelli D., Idiz E., Lyons T.W. and van den Boorn S.H.J.M. 2017. Molybdenum-isotope chemostratigraphy and paleoceanography of the Toarcian Oceanic Anoxic Event (Early Jurassic).

Fairbanks R.G., 1989. A 17,000-year glacio-eustatic sea level record—influence of glacial melting rates on the Younger Dryas event and deep-ocean circulation: Nature, 342, 637–641.

Fantasia A, Follmi K.B., Adatte T, Spangenberg J.E and Mattioli E. 2019. Expression of the Toarcian Oceanic Anoxic Event: new insights from a Swiss transect. Sedimentology, 66, 262–284.

Frimmel A., Oschmann W. and Schwark L. 2004. Chemostratigraphy of the Posidonia black shale, SW Germany I. Influence of sea level variation on organic facies evolution. Chem. Geol. 206, 199 – 230. Doi:10.1016/j.chemgeo.2003.12.007.

Gad M.A., Catt J.A. and Le Riche H.H. 1969. Geochemistry of the Whitbian (Upper Lias) sediments of the Yorkshire coast. Proc.Yorkshire Geol. Soc., 37(1), 105–140. doi: 10.1144/pygs.37.1.105

Guex J., Pilet S., Müntener O., Bartolini A., Spangenberg J., Schoene B., Sell B., and Schaltegger U. 2016. Thermal erosion of cratonic lithosphere as a potential trigger for mass-extinction. Sci. Reports, 6, 23168; doi: 10.1038/srep23168.

Hallam A. 1967. An Environmental Study of the Upper Domerian and Lower Toarcian in Great Britain. Phil. Trans. Royal Soc. London, Series B, 252(778), 393-445.

Hallam A. 1988. A re-evaluation of Jurassic eustasy in the light of new data and the revised Exxon curve. *In*: Wilgus, C.K. et al. (eds.) Sea-level Changes: an integrated approach. Society of Economic Paleontologists and Mineralogists, Special Publications, 42, 261–273.

Hallam A. 1997. Estimates of the amount and rate of sea-level change across the Rhaetian-Hettangian and Pliensbachian-Toarcian boundaries (latest Triassic to Early Jurassic). Jour. Geol. Soc. London, 154, 773–779.

Harries, P. J., and C. T. S. Little (1999). The Early Toarcian (Early Jurassic) and the Cenomanian-Turonian (Late Cretaceous) mass extinctions: Similarities and contrasts, Palaeogeogr. Palaeoclimatol. Palaeoecol., 154, 39–66.

Hesselbo, S.P., Gröcke D.R., Jenkyns H.C., Bjerrun C.J., Farrimond P., Morgans Bell H.S., Green O.R. 2000. Massive dissociation of gas hydrate during a Jurassic oceanic anoxic event. Nature 406, 392–395.

Hesselbo S.P., Jenkyns H.C., Duarte L.V. and Oliveira L.C.V. 2007. Carbon-isotope record of the Early Jurassic (Toarcian) Oceanic Anoxic Event from fossil wood and marine carbonate (Lusitanian Basin, Portugal). Earth Planet. Sci. Letters, 253, 455–470.

Howarth M.K. 1955, Domerian of the Yorkshire coast, Proc. Yorkshire Geol. Soc., 30, 147– 175.

Howarth M.K. 1962, The Jet Rock Series and the Alum Shale Series of the Yorkshire coast, Proc. Yorkshire Geol. Soc., **33**, 381–422.

Howarth M.K. 1973. The stratigraphy and ammonite fauna of the upper Liassic Grey Shales of the Yorkshire coast. Bull. Br. Mus. Nat. Hist. Geol. 24, 235–277.

Jenkyns H.C. 1988. The early Toarcian (Jurassic) anoxic event: stratigraphic, sedimentary, and geochemical evidence. Am. Jour. Sci., 288, 101–151.

Jenkyns H.C. 2010. Geochemistry of oceanic anoxic events. Geochem. Geophys. Geosyst. , 11, Q03004, doi:10.1029/2009GC002788.

Jochum J. 1993. Karbonatumverteilung, Mobilisation von Elementen und Migration von Erdöl-Kohlenwasserstoffen im Posidonienschiefer (Hildmulde, NW-Deutschland) in Abhängigkeit von der Palaötemperaturbeanspruchung durch das Massiv von Vlotho. Ber. Forsch. Juelich D82, 236 pp., Forsch. Juelich, Juelich, Germany.

Küspert W. 1982, Environmental changes during oil shale deposition as deduced from stable isotope ratios. *In* Cyclic and Event Stratification G. Einsele and A. Seilacher (eds), 482–501, Springer, Berlin.

Lézin C., Andreu B., Pellenard P., Bouchez J.-L., Emmanuel L., Fauré P., and Landrein P. 2013. Geochemical disturbance and paleoenvironmental changes during the Early Toarcian in NW Europe. Chemical Geology, 341, 1–15.

Little S.H., Vance D., Lyons T.W. and McManus J. 2015. Controls on trace metal authigenic enrichment in reducing sediments: insights from modern oxygen-deficient settings. American Journal of Science. 315(2), 77-119.

Little C.T.S. and Benton M.J. 1995. Early Jurassic mass extinction: a global long–term event. Geology, **23**, 495–498.

McArthur J.M., Donovan D.T., Thirlwall M.F., Fouke B.W. and D. Mattey 2000. Strontium isotope profile of the Early Toarcian (Jurassic) oceanic anoxic event, the duration of ammonite biozones, and belemnite palaeotemperatures. Earth Planet. Sci. Lett., 179, 269–285.Doi:10.1016/S0012-821X(00)00111-4.

McArthur J.M. (2007). Comment on “Carbon-isotope record of the Early Jurassic (Toarcian) Oceanic Anoxic Event from fossil wood and marine carbonate (Lusitanian Basin, Portugal)” by Hesselbo S., Jenkyns H.C., Duarte L.V. and Oliveira L.C.V. Earth PlanetLetters, (2007).

McArthur J.M., Algeo T.J., van de Schootbrugge, B., Li Q. and Howarth R.J. 2008. Basinal restriction, black shales, and the Early Toarcian (Jurassic) Oceanic Anoxic Event. Paleoceanography, **23**, PA4217, doi:10.1029/2008PA001607.

Neumann T, Christiansen C., Clasen S., Emeis K.-C. and Kunnzendorf H. 1997. Geochemical records of salt-water inflows into the deep basins of the Baltic Sea. Continental Shelf Research, 17(1), 95–115.

Neumeister S., Gratzer R., Algeo T.J., Bechtel A., Gawlick H.-J, Newton R.J. and Sachsenhofer R.F. 2016a. Oceanic response to Pliensbachian and Toarcian magmatic events: implications from an organic-rich basinal succession in the NW Tethys. Global Planet. Change, 126, 62-83.

Neumeister S., Algeo T.J Bechtel A., Gawlick H.-J. Gratzer R. and Sachsenhofer R.F. 2016b. Redox conditions and depositional environment of the Lower Jurassic Bachental bituminous marls (Tyrol, Austria). Austrian Journal of Earth Sciences, 109(2), 142-159.

Orani A.M., Vassileva E., Wysocka I., Angelidis M., Rozmaric M. and Louw D. 2018. Baseline study on trace and rare earth elements in marine sediments collected along the Namibian coast. Mar. Poll. Bull., 131, 386–395.

Page K.N. 2003. The Lower Jurassic of Europe: its subdivision and correlation, In Ineson J.R and Surlyk F. (eds.), Geological Survey of Denmark and Greenland Bulletin, 1, 23–59.

Page K.N. 2004. A sequence of biohorizons for the Subboreal Province Lower Toarcian in Northern Britain and their correlation with a Submediterranean Standard. Rivista Italiana di Paleontologia e Stratigrafia, 110, 109–114.

Page K.N. 2008. The evolution and geography of Jurassic ammonites. Proceedings of the Geologist's Association, 119, 35–57.

Pálfy J. and Smith P.L. 2000. Synchronony between Early Jurassic extinction, oceanic anoxic event, and the Karoo–Ferrar flood basalt volcanism. Geology, 28, 747–750.

Pearce C.R., Cohen A.S., Coe A.L. and Burton K.W. 2008. Molybdenum isotope evidence for global oceanic anoxia coupled with perturbations to the carbon cycle during the Early Jurassic, Geology, 36, 231–234.

Percival L.M.E., Witta M.L.I., Mather T.A., Hermoso M., Jenkyns H.C., Hesselbo S.P., Al-Suwaidi A.H., Storm M.S., Xu W. and Ruhl M. 2018. Globally enhanced mercury deposition during the end-Pliensbachian extinction and Toarcian OAE: a link to the Karoo–Ferrar Large Igneous Province. Earth Planet. Sci. Letters, 428, 267–280.

Piper D.Z. and Dean W.E. 2002. Trace-Element Deposition in the Cariaco Basin, Venezuela Shelf, under Sulfate-Reducing Conditions - a history of the local hydrography and global climate, 20 ka to the Present. U.S. Geological Survey Professional Paper 1670, 41pp.

Powell J. H. 1984. Lithostratigraphic nomenclature of the Lias Group in the Yorkshire Basin. Proceedings of the Yorkshire Geological Society, 45, 51–57.

Raup D.M. and Sepkoski J.J. 1984. Periodicity of extinctions in the geologic past. Proc. Nati. Acad. Sci., 81, 801-805.

Röhl H.-J., Schmid-Röhl A., Oschmann W., Frimmel A. and Schwark L (2001). The Posidonia Shale (lower Toarcian) of SW Germany: an oxygen depleted ecosystem controlled by sealevel and palaeoclimate. Palaeogeogr. Palaeoclimatol. Palaeoecol., 169, 273–299.

Rohling E.J., Marino G. and Grant K.M. 2015. Mediterranean climate and oceanography, and the periodic development of anoxic events (sapropels). Earth-Science Reviews 143, 62–97.

Saelen G., Doyle P. and Talbot M.R. 1996. Stable-isotope analyses of Belemnite rostra from the Whitby Mudstone Fm, England: surface water conditions during deposition of a marine black shale. Palaios, 11, 97–117.

Sælen G., Tyson R.V., Talbot M.R. and Telnæs N. 1998. Evidence of recycling of isotopically light CO2(aq) in stratified black shale basins; contrasts between the Whitby Mudstone and Kimmeridge Clay formations, United Kingdom. Geology, 26, 747–750.

Sælen G., Tyson R.V., Telnæs N. and Talbot M.R. 2000. Contrasting watermass conditions during deposition of the Whitby Mudstone (Lower Jurassic) and Kimmeridge Clay (Upper Jurassic) formations, UK. Palaeogeogr. Palaeoclimatol. Palaeoecol., 163, 163–196.

Schouten S., Van Kaam-Peters H.M.E., Rijpstra W.I.C., Schoell M.and Sinninghe Damsté J. S. (2000). Effects of an oceanic anoxic event on the stable carbon isotopic composition of Early Toarcian carbon. Am. J. Sci., 300, 1–22.

Schmid-Röhl A., Röhl H. Oschmann J. W., Frimmel A. and Schwark L. 2002. Palaeoenvironmental reconstruction of Lower Toarcian epicontinental black shales (Posidonia shale, SW Germany): global versus regional control. Geobios, 35, 13–20.

Scholz F., Baum M., Siebert C., Eroglu S. and Dale A.W. 2018. Sedimentary molybdenum cycling in the aftermath of seawater inflow to the intermittently euxinic Gotland Deep, Central Baltic Sea. Chem. Geol., 491, 27–38.

Schwark L. and A. Frimmel 2004. Chemostratigraphy of the Posidonia black shale, SW-Germany II. Assessment of extent and persistence of photic-zone anoxia using aryl isoprenoid distributions. Chem. Geol., 206, 231–248: doi : 10.1016 / j.chemgeo.2003.12.008.

Scott C. and Lyons T.W. 2012. Contrasting molybdenum cycling and isotopic properties in euxinic versus non-euxinic sediments and sedimentary rocks: refining the paleoproxies. Chemical Geology 324-325,19–27.

Simms M.J., Chidlaw N., Morton N. and Page K.N. 2004. British Lower Jurassic Stratigraphy. Geological Conservation Review Series No. 30, Joint Nature Conservation Committee, Peterborough, 458pp.

Sohlenius G., Sternbeck J., Andrén E. and Westman P. 1996. Holocene history of the Baltic Sea as recorded in a sediment core from the Gotland Deep. Marine Geology 134, 183-201.

Sohlenius G., Emeis K.-C., Andrén E., Andrén T., and Kohly A. 2001. Development of anoxia during the Holocene fresh-brackish water transition in the Baltic Sea. Marine Geology, 177, 221–242.

Suan G., Schöllhorn I., Schlögl J., Segit T. Mattioli E., Lécuyer C., Fourel F. and Mattioli E. 2018. Euxinic conditions and high sulfur burial near the European shelf margin (Pieniny Klippen Belt, Slovakia) during the Toarcian oceanic anoxic event. Global and Planetary Change, 170, 246–259.

Sweere S., van den Boorn S., Dickson A.J. and Reichart G.-J. 2016. Definition of new trace-metal proxies for the controls on organic matter enrichment in marine sediments based on Mn, Co, Mo and Cd concentrations. Chem. Geol, 441, 235–245.

Thibault N., Ruhl M., Ullmann C.V., Korte C., Kemp D.B., Gröcke D.R. and Hesselbo S.P. 2018. The wider context of the Lower Jurassic Toarcian oceanic anoxic event in Yorkshire coastal outcrops, UK. Proceedings of the Geologists' Association, 129, 372–391.

Thierry J. and Barrier E. 2000. Middle Toarcian. *In*: J. Dercourt, M. Gaetani, B. Vrielynck, E. Barrier, B. Biju-Duval, M.F. Brunet, J.P. Cadet, S. Crasquin and M. Sandulescu (Eds) . Atlas Peri-Tethys. Palaeogeographical Maps CCGM/CGMW, Paris.

van de Schootbrugge B., McArthur J.M., Bailey T.R., Rosenthal Y., Wright J.D., and Miller K.G. 2005. Toarcian oceanic anoxic event: An assessment of global causes using belemnite C isotope records. Paleoceanography, 20, PA3008, doi:10.1029/2004PA001102.

Wedepohl K. 1971. Environmental influences on the chemical composition of shales and clays. Phys. Chem. Earth 8, 305–333.

Wedepohl K. 1991. The composition of the upper Earth's crust and the natural cycles of selected metals. Metals in natural raw materials. Natural Resources, in Merian E. (ed), Metals and their compounds in the environment. Occurrence, analysis, and biological relevance. New York, VCH, p. 3–17.

Wignall P.B. 1991. Model for transgressive black shales. Geology, 19, 167–170.

Wignall P.B. and Hallam A. 1991. Biofacies, stratigraphic distribution and depositional models of British onshore Jurassic black shales. *In*: Tyson R.V. and Pearson T.H. (eds), 1991, Modern and Ancient Continental Shelf Anoxia. Geological Society Special Publication 58, 291–309.

Wignall P.B., Newton R.J. and Little C.T.S. 2005. The timing of paleoenvironmental change and cause-and-effect relationships during the Early Jurassic mass extinction in Europe. Am. J. Sci., 305, 1014–1032.

Wignall P.B. and Bond D.P.G. 2008. The end-Triassic and Early Jurassic mass extinction records in the British Isles. Proceedings of the Geologists' Association, 119(1), 73–84.

Wignall P.B., Bond D.P.G., Kuwahara K., Kakuwa Y., Newton R.J., and Poulton. S.W. 2010. An 80 million year oceanic redox history from Permian to Jurassic pelagic sediments of the Mino-Tamba terrane, SW Japan, and the origin of four mass extinctions. Global Planet. Change, 71, 109–123.

List of Figures

Fig. 1. Maps showing the positions of Yorkshire in relation to the disposition of land masses and organic-rich shales across NW Europe during Early Toarcian time. Maps modified from Suan *et al.* (2018) which, in turn, were modified from the palaeogeographic schemes of Thierry and Barrier (2000) and Dera *et al.* (2009).

Fig. 2. Element profiles through the uppermost Pliensbachian and the lower Toarcian sediments of the Cleveland Basin of Yorkshire. Concentrations recalculated to a calcite-free basis. Lithostratigraphy, ammonite zonation, and bed numbers are from Howarth (1955) for the Pliensbachian and Howarth (1962) for the Toarcian. Data for TOC and TS from McArthur *et al.* (2008). Data for $CaCO_3$, Cd, Co, Mn, and Mo, from this work.

Fig. 3. Profiles of palaeo-proxies Mo/TOC, Cd/Mo, and Co x Mn, through the uppermost Pliensbachian and lower Toarcian sediments of the Cleveland Basin, Yorkshire, UK. Profile of $\delta^{13}C$ from Cohen *et al.* (2004).

Fig. 4. Plot of element associations between TS, TOC, and $CaCO_3$ and the proxies Cd, Co, and Mn.

Fig. 5. Plot of Mo v Cd for shales from the Cleveland Basin, superimposed on the environmental fields of Sweere et al. (2016). Modified from their Fig. 4.

Fig. 6. Plot of Cd/Mo *v* Co(mg/kg)*Mn(%) for shales from the Cleveland Basin, superimposed on the environmental fields and data of Sweere *et al.* (2016); modified from Fig. 7b of those authors.

Fig. 7. The data for the Cleveland basin superimposed on the Co(mg/kg) × Mn(%) model and data of Sweere et al. (2016), who use a Co*Mn value of 0.4 to discriminate between restricted and unrestricted (upwelling) settings. Namibian data from Orani *et al.* (2018).

Fig. 8. a) The Co(EF)xMn(EF) model of Sweere et al. (2016) used to interpret depositional environments, based on a Co(EF)*Mn(EF) value of 1.0 (blue dotted line, range 0.5 to 2; elongate grey rectangle) to separate restricted from unrestricted environments. A more

appropriate field-divider is Co*Mn = 0.4 (black dotted curve), the divider used for Co*Mn (Fig. 7,– see text for an explanation). The divider of 0.4, rather than 1.0, better separates the Arkona Basin (Baltic, restricted) from the Arabian Sea (unrestricted/upwelling). Data from Sweere *et al.* (2016), Orani *et al.* (2018, Namibia). Average shale used as normalizer (Wedepohl 1971, 1991).

b), as in a) but with EFs calculated using local shales based on minimum local El/Al values. The restricted Arkona Basin (Baltic) overlaps with the Gulf of California.

List of Tables

Fig. 1.

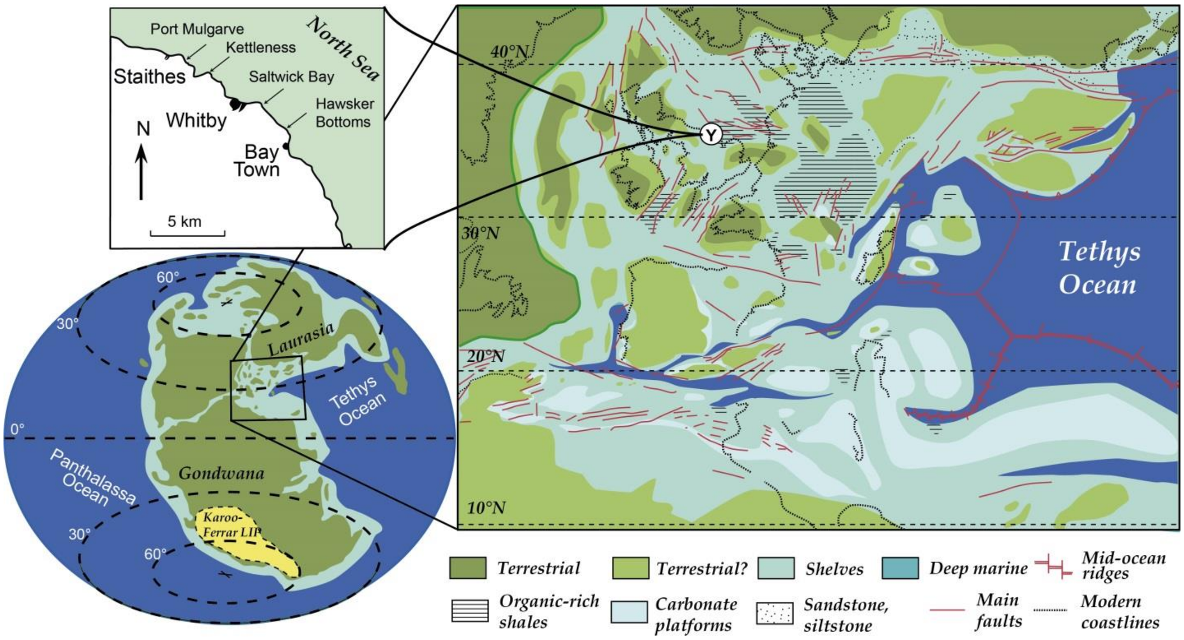

Fig. 1. Maps showing the positions of Yorkshire in relation to the disposition of land masses and organic-rich shales across NW Europe during Early Toarcian time. Maps modified from Suan *et al.* (2018) which, in turn, were modified from the palaeogeographic schemes of Thierry and Barrier (2000) and Dera *et al.* (2009).

Fig. 2.

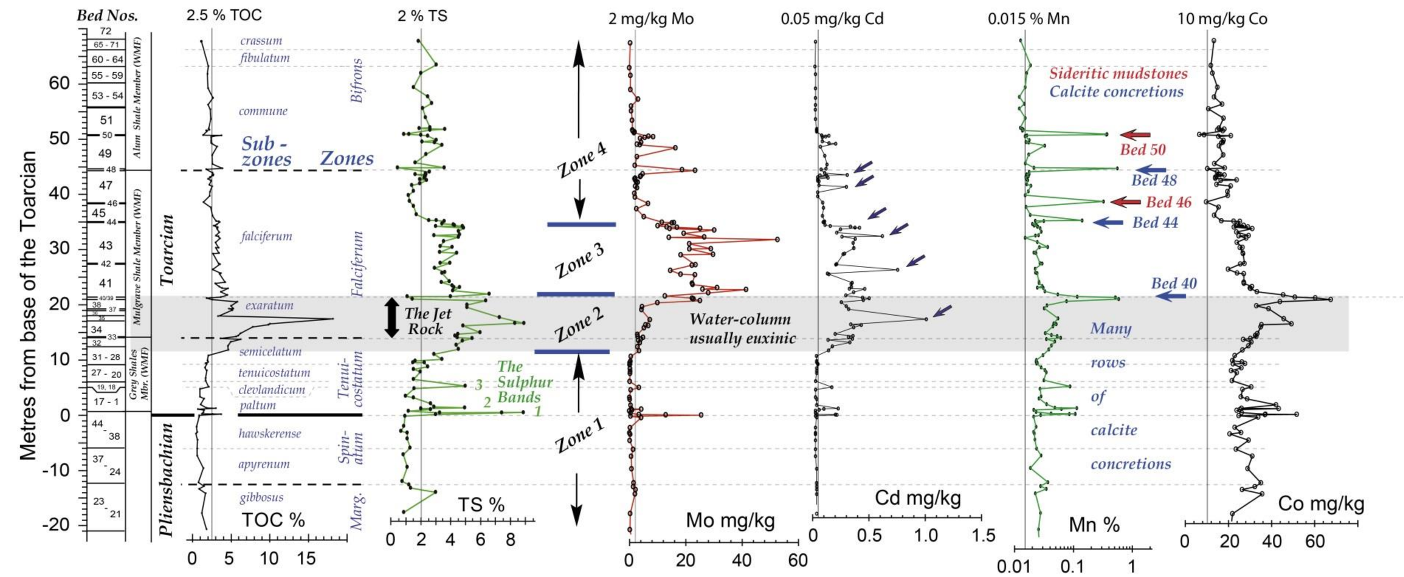

Fig. 2. Element profiles through the uppermost Pliensbachian and the lower Toarcian sediments of the Cleveland Basin of Yorkshire. Concentrations recalculated to a calcite-free basis. Lithostratigraphy, ammonite zonation, and bed numbers are from Howarth (1955) for the Pliensbachian and Howarth (1962) for the Toarcian. Data for TOC and TS from McArthur *et al.* (2008). Data for $CaCO_3$, Cd, Co, Mn, and Mo, from this work.

Fig. 3.

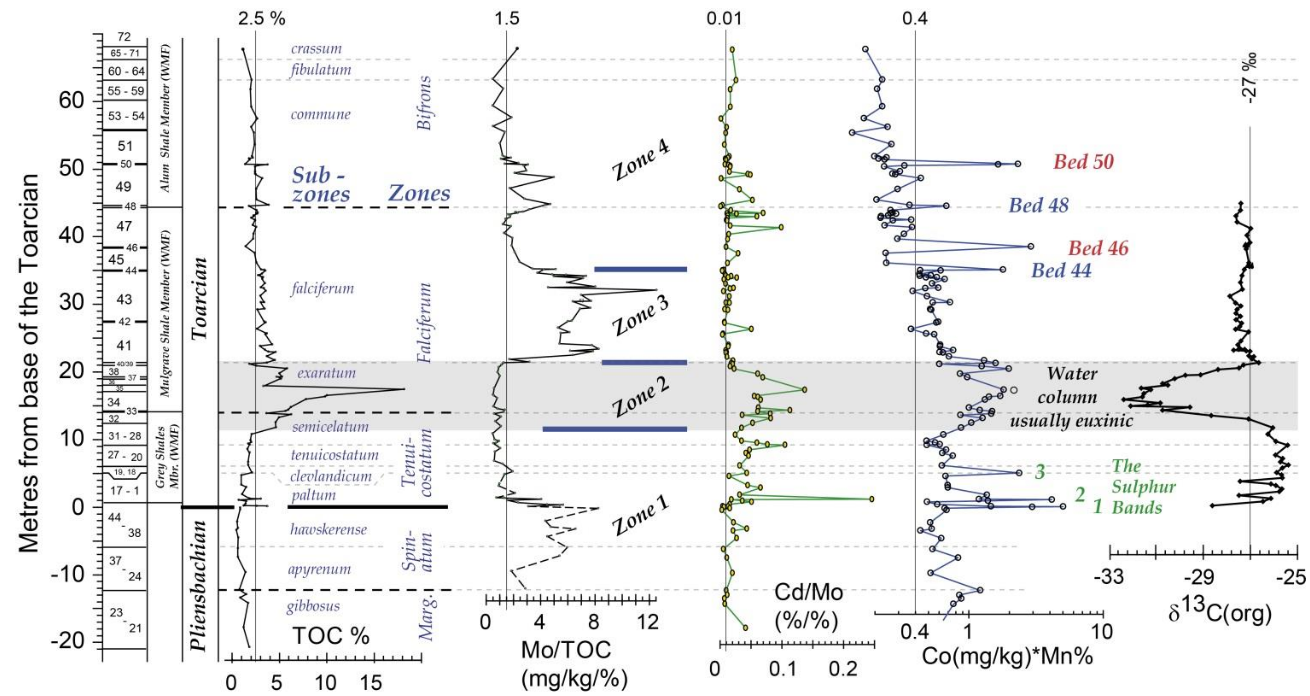

Fig. 3. Profiles of palaeo-proxies Mo/TOC, Cd/Mo, and Co x Mn, through the uppermost Pliensbachian and lower Toarcian sediments of the Cleveland Basin, Yorkshire, UK. Profile of $\delta^{13}C$ from Cohen *et al.* (2004).

Fig. 4.

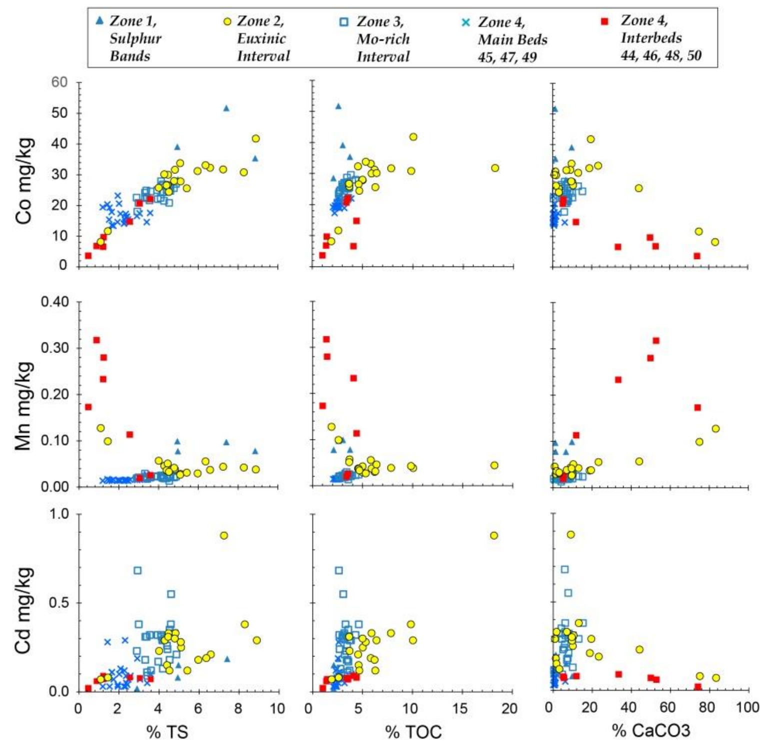

Fig. 4. Plot of element associations between TS, TOC, and $CaCO_3$ and the proxies Cd, Co, and Mn. For Mo relations, see McArthur *et al.* (2008).

Fig. 5.

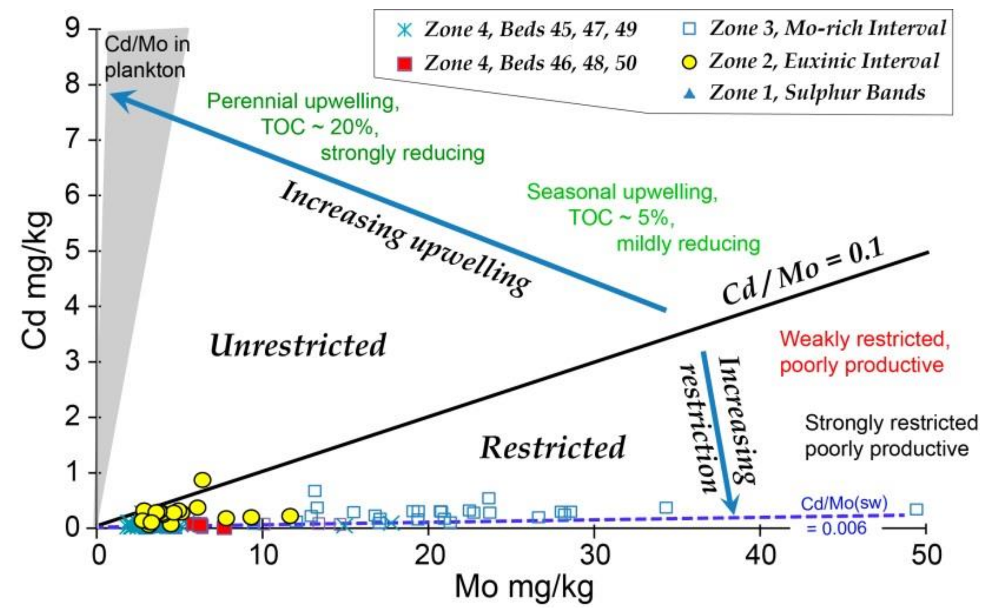

Fig. 5. Plot of Mo *v* Cd for shales from the Cleveland Basin, superimposed on the environmental fields of Sweere *et al.* (2016). Modified from their Fig. 4.

Fig. 6.

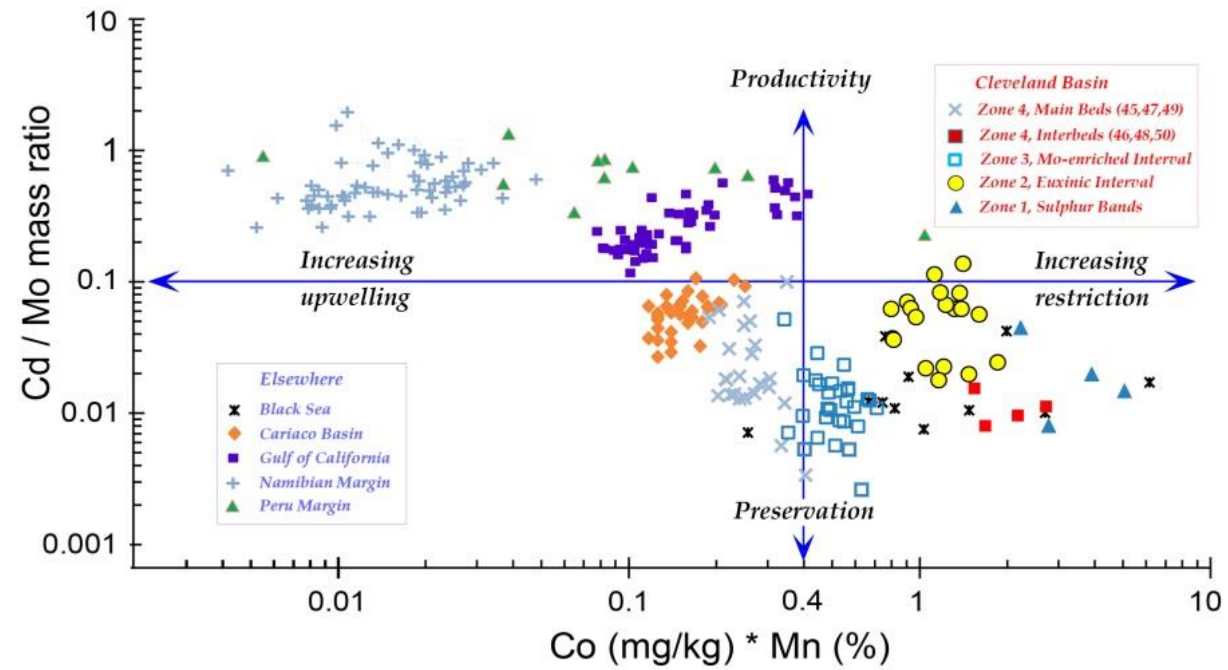

Fig. 6. Plot of Cd/Mo *v* Co(mg/kg)*Mn(%) for shales from the Cleveland Basin, superimposed on the environmental fields and data of Sweere et al. (2016); modified from Fig. 7b of those authors.

Fig. 7.

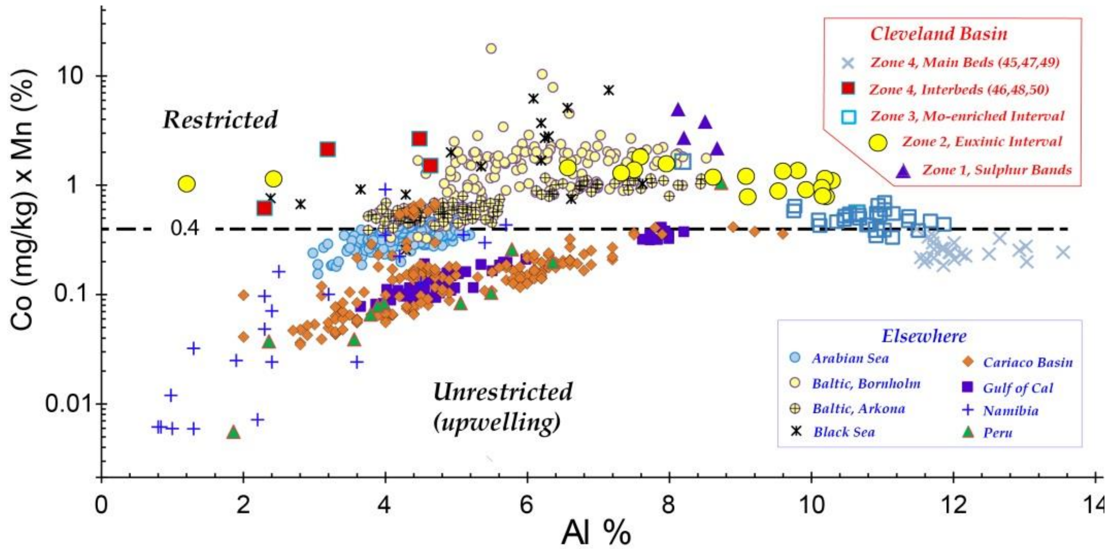

Fig. 7. The data for the Cleveland Basin superimposed on the Co(mg/kg) × Mn(%) model and data of Sweere *et al.* (2016), who use a Co*Mn value of 0.4 to discriminate between restricted and unrestricted (upwelling) settings. Namibian data from Orani *et al.* (2018).

Fig. 8.

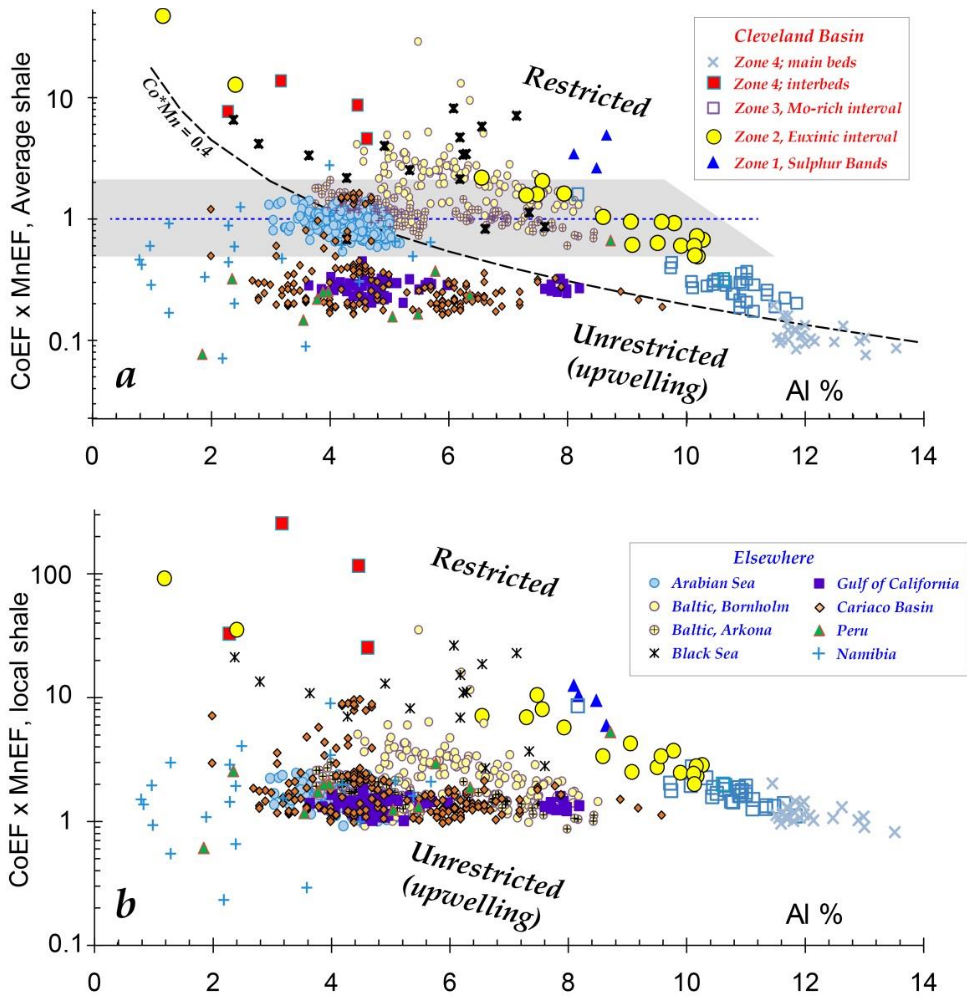

Fig. 8a) The Co(EF)*Mn(EF) model of Sweere *et al.* (2016) used to interprete depositional environments, based on a Co(EF)*Mn(EF) value of 1.0 (blue dotted line; range 0.5 to 2 shown as grey rectangle) to separate restricted from unrestricted environments. A more appropriate field-divider is Co*Mn = 0.4 (black dotted curve), the divider used for Co*Mn (Fig. 7, see text for an explanation). The divider of 0.4, rather than 1.0, better separates the Arkona Basin (Baltic, restricted) from the Arabian Sea (unrestricted/upwelling). Data from Sweere *et al.* (2016), Orani *et al.* (2018, Namibia). Average shale used as normalizer (Wedepohl 1971, 1991).

b), as in a) but with EFs calculated using local shales based on minimum local El/Al values. The Arkona Basin (restricted, Baltic) overlaps with the Gulf of California (slightly restricted(?), upwelling).

Table 1. Elemental composition of Toarcian shales from the Cleveland Basin of Yorkshire, UK.

Bed No	**Samp. No**	**Level m.a.d**	**TOC %**	**Al %**	**Cd mg/kg**	**Co mg/kg**	**Mn %**	**Mo mg/kg**
70	Y06-70	67.66	1.2	11.4	0.01	13.5	0.011	0.5
61	Y06-61	63.17	2.1	11.4	0.01	12.2	0.017	0.2
57	Y06-57	61.79	2.0	11.8	0.01	12.9	0.015	0.6
53 (No 3)	Y06-53/3	59.21	2.1	11.7	0.01	15.0	0.014	0.6
53 (No 2)	Y06-53/2	57.47	2.7	11.8	0.01	13.6	0.011	3.2
53 (No 1)	Y06-53/1	56.20	2.0	11.9	0.01	17.0	0.013	0.8
51 (No 3)	Y06-51/3	55.34	2.3	12.0	0.01	11.2	0.011	0.8
51 (No 2)	Y06-51/2	53.64	2.4	11.8	0.01	17.6	0.014	1.1
51	Li Y06/SB/51 (110/488)	51.87	2.1	13.8	0.02	15.7	0.011	1.2
51 (No 1)	Y06-51/1	51.67	2.2	12.0	0.02	17.9	0.012	1.4
51	Li Y06/SB/51 (75/488)	51.52	1.8	12.5	0.02	15.0	0.013	2.0
51	Li Y06/SB/51 (60/488)	51.37	1.9	12.3	0.02	17.3	0.012	1.8
50	Y06-50	50.72	1.4	3.2	0.06	6.8	0.317	6.3
50	Li Y06/SB/50 (0/13)	50.64	4.1	4.6	0.09	6.6	0.233	5.9
49 (No 4)	Y06-49/4	50.50	2.8	12.0	0.10	20.6	0.015	5.5
49	Li Y06/SB/49 (592/620)	50.36	2.5	12.0	0.07	15.5	0.014	3.9
49	Li Y06/SB/49 (519/620)	49.63	2.4	13.0	0.07	17.4	0.016	4.2
49 (No 3)	Y06-49/3	49.29	2.4	12.0	0.13	17.3	0.014	2.8
49	Li Y06/SB/49 (475/620)	49.19	2.5	12.9	0.19	16.6	0.016	3.7
49	Li Y06/SB/49 (420/620)	48.64	3.2	11.5	0.05	14.6	0.028	14.9
49 (No 2)	Y06-49/2	47.02	2.6	11.9	0.09	17.2	0.016	2.7
49 (No 1)	Y06-49/1	45.44	2.6	11.9	0.11	13.6	0.014	2.1
49	Li Y06/SB/49 (22/620)	44.66	3.9	12.6	0.10	17.6	0.019	17.8
49	Li Y06/SB/49 (9/620)	44.53	1.0	2.3	0.02	3.6	0.173	7.7
47	Li Y06/SB/47 (529/559)	43.90	2.6	12.5	0.09	14.8	0.016	4.7
47	Li Y06/SB/47 (492/559)	43.53	2.7	11.9	0.29	15.4	0.016	4.1
47	Li Y06/SB/47 (485/559)	43.46	2.6	12.1	0.05	16.2	0.015	3.9
47 (No 7)	Y06-47/7	43.39	2.7	11.7	0.11	17.9	0.015	3.9
47	Li Y06/SB/47 (451/559)	43.12	2.3	12.2	0.03	14.6	0.016	2.2
47	Li Y06/SB/47 (440/559)	43.01	2.3	13.0	0.12	14.2	0.014	2.0
47	Li Y06/SB/47 (416/559)	42.77	2.1	11.6	0.03	14.1	0.014	2.2
47 (No 6)	Y06-47/6	42.49	2.4	11.6	0.03	23.2	0.015	2.5
47	Li Y06/SB/47 (379/559)	42.40	2.4	13.5	0.04	16.4	0.015	3.1
47	Li Y06/SB/47 (307/559)	41.67	2.2	11.6	0.04	14.6	0.015	2.2
47 (No 5)	Y06-47/5	41.39	2.4	11.7	0.28	20.4	0.017	2.8
47 (No 4)	Y06-47/4	40.39	2.3	11.7	0.03	19.3	0.016	1.9
47 (No 3)	Y06-47/3	39.67	2.3	11.8	0.03	19.4	0.014	2.1
46	Y06-46	38.53	1.5	4.5	0.07	10	0.280	6.2
45 (No 1)	Y06-45/1	37.57	2.2	11.7	0.08	15	0.014	2.6
45 (No 2)	Y06-45/2	36.12	2.6	11.5	0.07	13	0.017	5.1
45	Li Y06/SB/45 (0/335)	35.12	4.4	8.2	0.08	15	0.113	10.0
44	Y06-44	35.04	3.4	10.9	0.08	21	0.019	14.6
44	Li Y06/SB/44 (3/15)	35.00	3.6	10.6	0.07	22	0.026	13.3
43	Li Y06/SB/43 (718/767)	34.48	3.2	11.5	0.09	22	0.017	9.5
43	LiY06/SB/43 (698/767)	34.28	2.8	11.7	0.13	24	0.020	12.0
43	LiY06/SB/43 (691/767) A	34.21	3.0	11.0	0.30	21	0.018	15.5

43	LiY06/SB/43 (671/767)	34.01	3.2	10.5	0.33	26	0.021	22.4
43 (No 4)	Y06-43/4	33.97	3.3	10.8	0.38	21	0.021	13.3
43	LiY06/SB/43 (641/767)	33.71	3.2	11.0	0.21	27	0.022	26.6
43	LiY06/SB/43 (580/767) A	33.10	3.5	10.1	0.18	21	0.023	17.1
43	LiY06/SB/43 (515/767)	32.45	3.1	10.9	0.55	26	0.021	23.6
43 (No 3)	Y06-43/3	32.37	3.4	10.1	0.23	23	0.019	12.9
43 (No 6)	Y06-43/6	31.97	3.6	10.9	0.35	26	0.013	49.3
43	LiY06/SB/43 (392/767)	31.22	2.7	11.9	0.32	22	0.021	19.4
43 (No 5)	Y06-43/5	30.30	3.4	10.9	0.31	23	0.029	28.0
43	LiY06/SB/43 (307/767)	30.27	3.1	10.5	0.32	22	0.022	19.1
43 (No 2)	Y06-43/2	29.30	3.5	10.3	0.26	25	0.019	28.2
43	LiY06/SB/43 (200/767)	29.20	2.7	11.4	0.24	24	0.020	16.8
43 (No 1)	Y06-43/1	27.40	3.4	10.7	0.18	24	0.022	20.9
43	LiY06/SB/43 (2/767)	27.32	3.6	11.4	0.17	22	0.024	19.4
SB 41 (No 2)	Y06-41/2	26.37	2.6	11.1	0.68	18	0.019	13.2
PM-10J	41 (438/587)	25.68	3.0	10.8	0.11	22	0.020	17.0
SB 41 (1)	Y06-41/1	25.57	3.2	10.7	0.12	25	0.021	21.3
HB 41 (272/587)	Y07 HB GS	24.02	3.7	10.9	0.32	25	0.022	20.7
HB 41 (250/587)	Y07 HB GS	23.80	3.0	11.1	0.31	25	0.022	20.8
HB 41 (195/587)	Y07 HB GS	23.25	3.5	11.0	0.31	28	0.025	28.5
41 (165/587)	Y07 PM	22.95	3.8	10.5	0.29	27	0.021	23.7
41 (160/587)	Y07 PM	22.90	4.6	9.7	0.38	25	0.024	34.3
41 (100/587)	Y07 PM	22.30	3.7	9.8	0.29	26	0.025	22.7
41 (43/587)	Y07 PM	21.73	4.6	8.6	0.21	32	0.037	9.3
41 (2/587)	Y07 PM	21.33	3.3	6.6	0.23	26	0.057	11.7
40 (20/30)	Y07 PM	21.20	1.4	1.2	0.07	8	0.128	3.2
39 (12/23)	Y07 PM	20.88	1.9	2.4	0.08	12	0.099	4.5
38 (126/152)	Y07 PM	20.50	5.8	7.6	0.19	33	0.056	7.8
38 (53/152)	Y07 PM	19.77	5.0	9.1	0.25	28	0.028	4.0
38 (0/152)	Y07 PM	19.24	5.3	9.5	0.28	34	0.027	4.0
35 (45/91)	Y07 PM	17.41	18.2	7.5	0.88	38	0.044	6.4
HB34 (212/259)	Y07 HB GS	16.49	10.1	7.9	0.29	42	0.038	5.1
34 (199/259)	Y07 PM	16.36	9.8	7.3	0.38	31	0.042	6.1
34 (158/259)	Y07 PM	15.95	7.8	9.1	0.33	32	0.039	4.9
K34 (38/259)	Y07 Kettleness GS	14.75	5.7	9.9	0.18	31	0.030	2.9
K34 (2/259)	Y07 Kettleness GS	14.39	5.2	10.3	0.33	30	0.037	2.9
PM33 (0/15)	Y07 PM	14.22	5.7	9.8	0.29	30	0.046	4.7
PM32 (148/183)	Y07 PM GS	13.88	3.7	9.6	0.31	27	0.051	3.8
K32 (128/183)	Y07 Kettleness GS	13.67	6.3	10.2	0.12	26	0.031	3.2
K32 (83/183)	Y07 Kettleness GS	13.22	5.0	10.2	0.30	28	0.042	3.6
K32 (13/183)	Y07 Kettleness GS	12.52	4.6	10.1	0.15	27	0.036	2.8
K31 (152/213)	Y07 Kettleness GS	11.78	4.7	10.1	0.12	24	0.033	3.3
	HB NSB-44b	10.76	1.7	10.6	0.02	22	0.027	0.7
K29 (77/107)	Y07 Kettleness GS	9.86	2.0	11.1	0.02	21	0.021	0.6
PM29 (50/107)	Y07 PM GS	9.60	2.1	11.0	0.02	25	0.021	0.3
K29 (25/107)	Y07 Kettleness GS	9.34	1.7	11.3	0.03	26	0.022	0.4
	HB NSB-42a	9.26	1.9	11.2	0.03	21	0.021	0.3
PM27 (29/61)	Y07 PM GS	8.55	1.6	11.0	0.02	25	0.025	0.4
PM25 (45/61)	Y07 PM GS	8.05	1.9	10.7	0.02	20	0.029	0.5
HB NSB	HB NSB-40b	7.66	1.7	10.6	0.02	23	0.031	0.4
PM20 (7/15)	Y07 PM GS	6.22	1.7	10.8	0.01	21	0.028	0.3
	HB NSB-39	5.11	2.1	8.7	0.15	28	0.078	3.4

PM18 (17/38)	Y07 PM GS	4.67	1.2	11.2	0.01	25	0.024	0.6
	HB NSB-28	3.31	1.3	11.2	0.01	25	0.026	0.2
PM8 (15/41)	Y07 PM GS	2.95	1.4	11.1	0.02	27	0.023	0.3
PM4 (11/36)	Y07 PM GS	1.89	1.1	10.5	0.02	40	0.032	0.6
HB2 (8/53)	Y07 HB GS	1.25	1.9	11.0	0.21	25	0.044	0.9
No. 2/53	HB NSB-19	1.19	3.0	8.5	0.08	39	0.099	4.0
PM1 (36/51)	Y07 PM GS	1.02	0.7	10.3	0.04	24	0.055	1.1
	HB NSB-18	0.86	1.5	11.0	0.01	23	0.019	0.2
HB43 (66/76)	Y07 HB ML	0.48	1.4	11.6	0.01	25	0.021	0.6
HB43 (38/76)	Y07 HB ML	0.20	1.3	10.2	0.02	36	0.038	3.5
	HB NSB-15	0.15	2.6	8.1	0.19	48	0.097	12.6
PM26 (10/15)	Y07 PM GS	0.10	3.7	8.2	0.20	35	0.078	25.0
	HB NSB-14	-0.09	0.9	10.6	0.01	24	0.025	0.6
PM57 (78/113)	Y07 PM ML	-0.36	0.9	10.9	0.02	33	0.019	4.3
	HB NSB-8a	-2.19	0.6	11.3	0.01	22	0.021	0.4
HB38 (170/208	Y07 HB ML	-3.13	0.7	10.9	0.01	25	0.019	0.2
	HB NSB-6	-3.39	0.5	10.6	0.01	20	0.020	0.4
HB38 (32/208)	Y07 HB ML	-4.51	0.7	10.9	0.01	28	0.020	0.3
HB34 (55/137)	Y07 HB ML	-6.13	0.7	11.0	0.01	23	0.022	1.4
HB32 (51/96)	Y07 HB ML	-7.39	0.6	10.9	0.01	30	0.026	0.8
HB28 (90/165)	Y07 HB ML	-9.65	1.0	11.6	0.02	28	0.017	0.9
PM38 (134/170)	Y07 PM ML	-12.22	0.8	9.4	0.02	34	0.033	1.7
St38 (66/170)	Y07 Staithes ML	-12.90	1.5	10.1	0.02	31	0.025	1.5
PM38 (13/170)	Y07 PM ML	-13.43	0.9	9.7	0.02	26	0.032	2.3
St36 (50/112)	Y07 Staithes ML	-14.23	1.7	10.2	0.02	34	0.021	2.1
St34 (61/340)	Y07 Staithes ML	-17.78	1.2	10.4	0.02	21	0.025	0.5
St30 (31/51)	Y07 Staithes ML	-20.72	1.9	11.0	0.08	20	0.023	0.4
St27 (386/579)	Y07 Staithes ML	-23.09	0.5	9.4	0.03	31	0.024	1.3
St27 (2/579)	Y07 Staithes ML	-26.93	0.9	11.1	0.02	23	0.018	0.6
St25 (56/249)	Y07 Staithes ML	-28.95	0.7	10.5	0.02	23	0.020	1.3
St17 (385/564)	Y07 Staithes ML	-35.19	0.3	9.7	0.01	19	0.018	1.6
Measured								
BCR 701 Lake Sediment (extractables)					11.19	15.8		4.03
MAG-1, Marine Sediment					0.25	26.3		1.57
SGR-1, Green River Shale					1.08	12.2		35.6
SCo-1, Cody Shale					0.20	13.1		1.50
Accepted Value (Gladney E.S. & Roelandts I., 1988, except BRC 701)								
BCR 701 Lake Sediment (extractables)					11.3	–		–
MAG-1, Marine Sediment					0.20	20.4		1.60
SGR-1, Green River Shale					0.93	11.8		35.1
SCo-1, Cody Shale					0.14	10.5		1.37

Gladney E.S. & Roelandts I., 1988
1987 Compilation of elemental concentration
data for USGS BHVO-1, MAG-1, QLO-1,
RGM-1, SCO-1, SDC-1, SGR-1 AND STM-1
Geostandards Newsletter, 12(2),1988, 253-362

1138